Performance and Biodegradability of a Maleated Polyester Bioplastic/Recycled Sugarcane Bagasse System

Chin-San Wu

Department of Chemical and Biochemical Engineering, Kao Yuan University, Kaohsiung County, Taiwan 82101, Republic of China

Received 3 February 2010; accepted 26 August 2010
DOI 10.1002/app.33713
Published online 22 February 2011 in Wiley Online Library (wileyonlinelibrary.com).

ABSTRACT: The biodegradability, morphology, and mechanical properties of composite materials made of poly(butylene succinate adipate) (PBSA) and sugarcane bagasse (SCB) were evaluated. Composites containing maleic anhydride (MA)-grafted PBSA (PBSA-*g*-MA/SCB) exhibited noticeably superior mechanical properties because of greater compatibility between the two components. The dispersion of SCB in the PBSA-*g*-MA matrix was highly homogeneous as a result of ester formation between the carboxyl groups of PBSA-*g*-MA and hydroxyl groups in SCB and the consequent creation of branched and crosslinked macromolecules. Each composite was subjected to biodegradation tests in a *Rhizopus oryzae* compost. Morphological observations indicated severe disruption of film structure after 60 days of incubation, and both the PBSA and the PBSA-*g*-MA/SCB composite films were eventually completely degraded. The PBSA-*g*-MA/SCB films were more biodegradable than those made of PBSA and exhibited a higher intrinsic viscosity, implying a strong connection between these characteristics and biodegradability. © 2011 Wiley Periodicals, Inc. J Appl Polym Sci 121: 427–435, 2011

Key words: poly(butylene succinate adipate); biodegradation; sugarcane bagasse

INTRODUCTION

Recently, awareness of the environmental damage caused by nonbiodegradable plastics has increased. Although recycling is an environmentally attractive solution, only a small percentage of plastics are actually recyclable and most end up in municipal landfills. This awareness has led to a great deal of research aimed at producing ecofriendly polymers, and considerable interest has emerged in the production and use of materials that are renewable, degradable, and recyclable, better known as "green materials."[1–5]

Among the commercialized biodegradable plastics, poly(butylene succinate adipate) (PBSA) has received a great deal of attention because of its mechanical strength, hydrophobic nature, and biodegradability.[6,7] However, high production costs appear to limit its commercial applications. This limitation can be overcome by blending PBSA with cost-effective, biodegradable, natural biopolymers such as starch, cellulose, or natural fibers to create new materials with improved physical properties.[8–11] Creating composites of PBSA and natural fibers markedly reduces costs and enables tailoring of the biodegradability and mechanical properties of the hybrid products. Natural fiber such as sugarcane bagasse (SCB) is one of the most available and renewable resources that represent a promising low-cost raw material.[12] However, because natural fibers are fairly hydrophilic, poor compatibility between the two phases often requires the addition of a compatibilizer to obtain acceptable mechanical properties.[13] Maleated polyester copolymer has been demonstrated as an effective compatibilizer in polyester/natural fiber composites,[14] and coupling agents have been used to increase the compatibility between polyester and plant fibers.[15]

Many new materials created by blending biodegradable polymers with natural fibers have demonstrated complete degradation in soil or compost without the emission of any toxic or noxious components. As a result, several biodegradable polymers such as PBSA, poly(butylene succinate), and poly(lactic acid) have become of increasing commercial interest. As opposed to conventional plastics such as polystyrene (PS) and polyethylene, which require hundreds or even thousands of years to degrade, PBSA can degrade into naturally occurring products in just a few years.[16] PBSA is also noted for its flexibility and can be produced by polymerization of glycols with dicarboxylic acids.[17] As a result, PBSA has been used in composites with other polymers as a packaging material and has been proposed for use in biomedical applications.[18] As with other aliphatic polyesters,[19] the biocompatibility of PBSA and its copolymers has led to several commercially successful applications.

Correspondence to: C.-S. Wu (cws1222@cc.kyu.edu.tw).

© 2011 Wiley Periodicals, Inc.

Unfortunately, PBSA is relatively expensive. One way to reduce the cost of PBSA-based materials is by blending with natural biomaterials. Dried SCB has been combined with thermoplastic composites, but SCB ranging in length from millimeters to a centimeter does not mix well in polyester matrices and requires a compatibilizing agent to wet the fibers. The wettability of adhesion of PBSA and SCB is important in getting of a strong and durable bond, because it allows an intimate molecular contact at the interface.[20] The higher hydrophilicity of PBSA results in a natural wetting of SCB. Composites of PBSA and SCB, therefore, offer advantages in both biocompatibility and cost.[21] SCB is a renewable, cellulosic, agroindustrial byproduct of the sugar and alcohol industry with a short regeneration cycle. Although much of the baggase produced by sugarcane processing is used to fuel its own production, the remaining bagasse is still an environmental burden. Any explorations of novel applications of SCB would be of great significance.[22,23] For this reason, the development of high-performance natural fiber composite materials incorporating SCB has become a popular research topic worldwide.

This report describes a systematic investigation of the mechanical properties and biodegradability of SCB composites with PBSA and maleic anhydride (MA)-grafted PBSA (PBSA-*g*-MA). The composites were characterized using Fourier transform infrared spectroscopy (FTIR) and ^{13}C-nuclear magnetic resonance (NMR) to identify bulk structural changes induced by the MA moiety. In addition, the effects of SCB content on biodegradability were assessed for both the PBSA/SCB and PBSA-*g*-MA/SCB composites.

EXPERIMENTAL

Microbiological sample preparation

Rhizopus oryzae (ATCC9363) was supplied by the Bioresource Collection and Research Center in Taiwan. The strain was cultivated at 30°C and stirred at 120 rpm in a medium consisting of 1.5 g malt extract powder, 1.5 g glucose, and 150 mL distilled water at pH 7.0 ± 0.5. The culture was collected in its early stationary phase for cell entrapment.

Materials

Poly(butylene succinate adipate) was supplied by Mitsubishi Chemical (Tokyo, Japan). Maleic anhydride, obtained from Sigma (St. Louis, MO), was purified before use by recrystallization from chloroform. Benzoyl peroxide (BPO; Sigma) was used as an initiator and was purified by dissolution in chloroform and reprecipitation in methanol. SCB was obtained from Pingtung.

PBSA-*g*-MA copolymer

MA was grafted onto PBSA dissolved in tetrahydrofuran under a nitrogen atmosphere (100% of N_2) at 50°C ± 2°C, and the polymerization reaction was initiated with 0.3 wt % BPO. The reaction system was stirred at 60 rpm for 8 h. The grafted product (4 g) was then dissolved in 200 mL of refluxing tetrahydrofuran at 50°C ± 2°C, and the hot solution was filtered through several layers of cheesecloth. The cheesecloth was washed with 600 mL of acetone to remove the tetrahydrofuran-insoluble, unreacted MA, and the remaining product was dried in a vacuum oven at 80°C for 24 h. The tetrahydrofuran-soluble component of the filtrate was extracted five times using 600 mL of cold acetone for each extraction. Subsequently, the grafting percentage was determined using a titration method.[24]

Determination of grafting percentage

MA loading of the tetrahydrofuran-soluble polymer (expressed as grafting percentage) was calculated from the acid number and was determined as follows. First, about 2 g of copolymer was heated in 200 mL of refluxing tetrahydrofuran for 2 h. The hot solution was then titrated immediately with a 0.03*N* ethanolic KOH solution, which was standardized against a solution of potassium hydrogen phthalate, with phenolphthalein used as an indicator. The acid number was calculated using eq. (1) below, and the grafting percentage was calculated using eq. (2).[24]

$$\text{Acid number (mg KOH/g)} = \frac{V_{\text{KOH}}\ (\text{mL}) \times C_{\text{KOH}}(N) \times 56.1}{\text{polymer (g)}} \quad (1)$$

$$\text{Grafting percentage (\%)} = \frac{\text{Acid number} \times 98.1}{2 \times 561} \times 100\%. \quad (2)$$

Grafting percentage was found to be about 1.12 wt % when BPO loading was maintained at 0.3 wt % and MA loading was maintained at 10 wt %.

SCB processing

SCB was extracted from crushed Taiwanese sugarcane. Purification consisted of immersing 50 g of ground and dried SCB in 1000 mL of distilled water to remove any water-soluble components. After 3 days, the suspension was filtered, and 1000 mL of NaOH (0.25*M*) was added to the SCB. After 24 h, this mixture was vacuum filtered. The bagasse was refluxed in three successive portions of 20% (v/v) nitric acid solution in ethanol; the solution was replaced every 2 h. After refluxing, the mixture was filtered and washed with distilled water until no yellowing was observed when

phenolphthalein and a drop of NaOH (0.05*M*) were added to it. The bagasse was dried at 60–70°C for 48 h and then ground in a blender. The samples were processed through 42-mesh (0.351 mm) and 60-mesh (0.246 mm) sieves, air dried for 24 h at 60–70°C, and vacuum dried for at least 3 h at 105°C until the moisture content fell to 3% ± 1%.

Composite preparation

Before composite fabrication, SCB samples were cleaned with acetone and dried in an oven at 105°C for 24 h. Composites were prepared in a "Plastograph" 200-Nm Mixer W50EHT with a blade rotor (Brabender, Dayton, OH). The composites were mixed between at 100 and 110°C for 15 min at a rotor speed of 50 rpm. Samples were prepared with mass ratios of SCB to PBSA or to PBSA-*g*-MA of 5/95, 10/90, 15/85, and 20/80. Residual MA in the PBSA-*g*-MA reaction mixture was removed via acetone extraction before the preparation of PBSA-*g*-MA/SCB. After mixing, the composites were pressed into thin plates with a hot press and placed in a dryer for cooling. These thin plates were cut to standard sample dimensions for further characterization.

NMR/FTIR/XRD analyses

Solid-state ^{13}C-NMR analysis was performed with an AMX-400 NMR spectrometer and was obtained at 100 MHz under cross polarization while spinning at the magic angle. Power decoupling conditions were set with a 90° pulse and a 4-s cycle time. Infrared spectra of the samples were obtained using a Bio-Rad FTS-7PC FTIR spectrophotometer. X-ray diffraction (XRD) data were recorded using a Rigaku D/max 3V X-ray diffractometer with a Cu target and a K_α source at a scanning rate of 2°/min. Melting temperature (T_m) and fusion heat (ΔH_f) were determined via a TA instrument 2010 DSC system. For the DSC tests, sample weight ranged at 4–6 mg and temperature of −30°C ± 120°C, with a heating rate of 10°C/min, whereas GPC was performed using a Perkin Elmer Series 200 system (Waltham, MA) at 40°C. Chloroform was used as the effluent (flow rate 1.0 mL/min) during the GPC analysis. Gel DVB 10000As (Jordi, Bellingham, MA) was used as the gel columns with an RI-71 (Shodex, Tokyo, Japan) as a detector and PS as the standard.

Composite morphology

A thin film of each composite was created with a hydrolytic press and treated with hot water at 80°C for 24 h before being coated with gold. The surface morphology of these thin films was observed using a scanning electron microscope (SEM, Hitachi Microscopy Model S-1400, Tokyo, Japan).

Exposure to *R. oryzae*

Samples were cast into films using a 30 × 10-mm plastic mold. Films were removed from the mold and rinsed several times with distilled water until the waste water had a neutral pH. The films were then clamped to a glass sheet and dried in a vacuum oven (50°C ± 2°C, 66.7 Pa, 24 h). After drying, the films were 0.05 ± 0.02-mm thick.

The dried films were placed in compost Petri dishes containing 30 mL of NB broth and *R. oryzae* ATCC9363 and incubated at pH 7.0 ± 0.5, 30°C ± 2°C, and 50% ± 5% relative humidity. After incubation, the films were washed extensively with deionized water and dried. Each study was conducted using three replicate test reactors and three replicate samples in each test reactor. Each result is therefore based on nine samples.

Intrinsic viscosity

A Schott capillary viscometer was used to measure the intrinsic viscosity of PBSA and PBSA-*g*-MA/SCB dissolved at various concentrations (0.5, 1.0, 1.5, and 0.2 g/dL) in a chloroform solvent. Solutions were then cleared through a 0.45-μm filter (Lida Manufacturing, Kenosha, WI). Subsequently, the capillary viscometer was filled with a 10-mL sample and equilibrated in a water bath (Schott B801, Gruenplan, Germany) at 30°C ± 0.5°C. Each sample was passed through the capillary tube once before the flow time was measured. The flow time was used to calculate the relative viscosity and the reduced viscosity. The reduced viscosity was plotted as a function of PBSA or PBSA-*g*-MA/SCB concentration, with the *y*-intercept determining the intrinsic viscosity.

RESULTS AND DISCUSSION

FTIR/NMR analysis

FTIR spectra of unmodified PBSA and PBSA-*g*-MA are shown in Figure 1(A,B), respectively. The characteristic transitions of PBSA at 3300–3700, 1700–1760, and 500–1500 cm^{-1} were appeared in the spectra of both polymers, with two extra shoulders observed at 1785 and 1857 cm^{-1} in the modified PBSA spectrum. These features are characteristic of anhydride carboxyl groups. Similar results have been reported previously.[25,26] The shoulders represent free acid in the modified polymer and therefore denote the grafting of MA onto PBSA. The SCB FTIR spectrum [Fig. 1(E)] exhibited peaks at 3253 and 1072 cm^{-1} attributable to hydroxyl groups and —CO stretching, respectively.[27]

The peak assigned to the O—H stretching vibration at 3200–3700 cm^{-1} was intensified in the PBSA/SCB (20 wt %) composite [Fig. 1(C)] because of

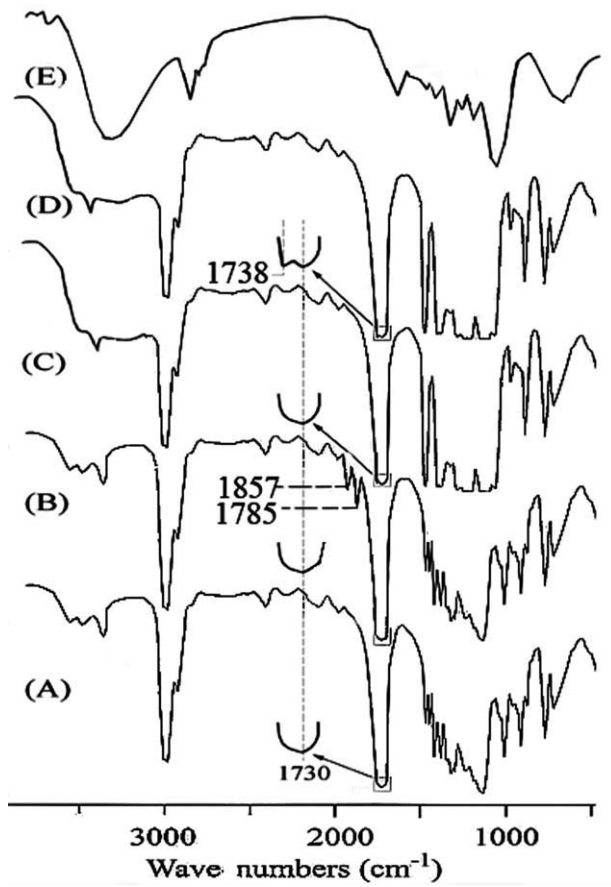

Figure 1 FTIR spectra are given for (A) PBSA, (B) PBSA-*g*-MA, (C) PBSA/SCB (20 wt %), (D) PBSA-*g*-MA/SCB (20 wt %), and (E) SCB.

contributions from the —OH group of SCB. The FTIR spectrum of the PBSA-*g*-MA/SCB (20 wt %) composite in Figure 1(D) revealed a peak at 1738 cm^{-1} that was not present in the FTIR spectrum of the PBSA/SCB (20 wt %) composite. This peak was assigned to the ester carbonyl stretching vibration of the copolymer. Yoshimura et al.[28] also reported an absorption peak at 1735 cm^{-1} for this ester carbonyl group. These data suggest the formation of branched and crosslinked macromolecules in the PBSA-*g*-MA/SCB composite by a covalent reaction of the anhydride carboxyl groups in PBSA-*g*-MA with the hydroxyl groups of SCB.

To further confirm this finding, solid-state ^{13}C-NMR spectra of PBSA and PBSA-*g*-MA are compared in Figure 2(A,B), respectively. Six peaks were observed corresponding to carbon atoms in the unmodified PBSA (1,2: δ = 24.6 ppm; 3: δ = 27.7 ppm; 4: δ = 33.6 ppm; 5: δ = 63.2 ppm; 6: δ = 171.3 ppm; and 7: δ = 172.7 ppm).[17] The ^{13}C-NMR spectrum of PBSA-*g*-MA showed additional peaks (8: δ = 36.2 ppm; 9: δ = 42.3 ppm; and 10: —C=O δ = 174.5 ppm), thus confirming that MA was grafted covalently onto PBSA.

The solid-state ^{13}C-NMR spectra of PBSA/SCB (20 wt %), PBSA-*g*-MA/SCB (20 wt %), and SCB are shown in Figure 2(C–E). Relative to unmodified PBSA, additional peaks located at δ = 36.2 ppm (8) and δ = 42.3 ppm (9) were observed in the spectra of composites containing PBSA-*g*-MA. These same features were observed in previous studies[29] and indicate grafting of MA onto PBSA. However, the peak at δ = 174.5 ppm (C=O) (10) [Fig. 2(B)], which is also typical for MA grafted onto PBSA, was absent in the solid-state PBSA-*g*-MA/SCB spectrum (20 wt %). This occurrence was most likely the result of an additional condensation reaction between the anhydride carboxyl group of MA and the —OH group of SCB that caused the peak at δ = 173.7 ppm to split into two bands (11: δ = 176.3 ppm and 12: δ = 177.2 ppm). This additional reaction converted the fully acylated groups in the original SCB to esters [represented by peaks 11 and 12 in Fig. 3(C)] and did not occur between PBSA and SCB, as indicated by the absence of corresponding peaks in the NMR spectrum of PBSA/SCB (20 wt %) [Fig. 2(D)]. The formation of ester groups significantly affects the thermal and biodegradation properties of PBSA-*g*-MA/SCB

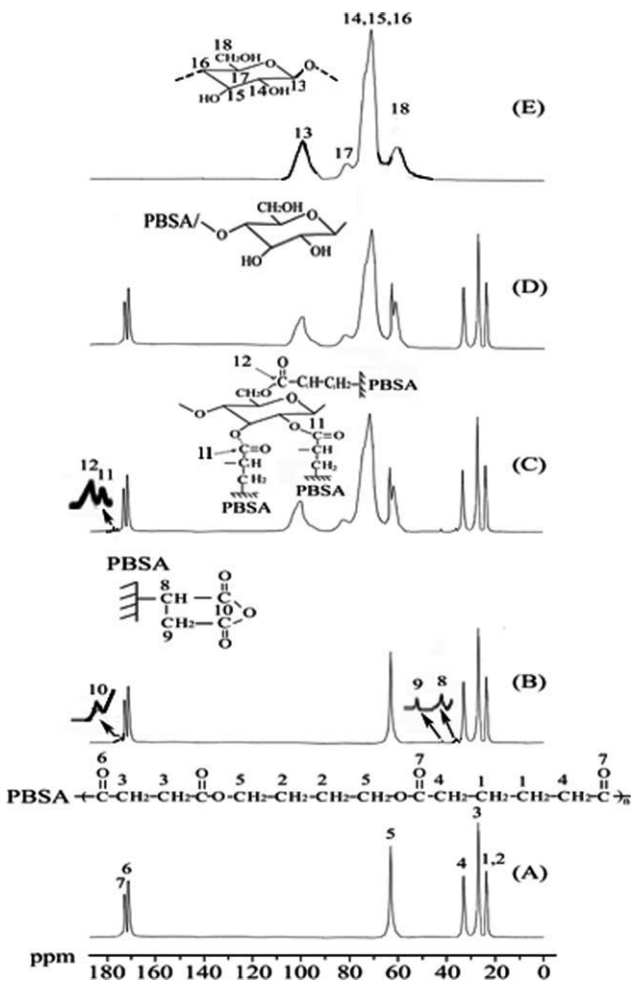

Figure 2 Solid-state ^{13}C-NMR spectra are shown for (A) PBSA, (B) PBSA-*g*-MA, (C) PBSA/SCB (20 wt %), (D) PBSA-*g*-MA/SCB (20 wt %), and (E) SCB.

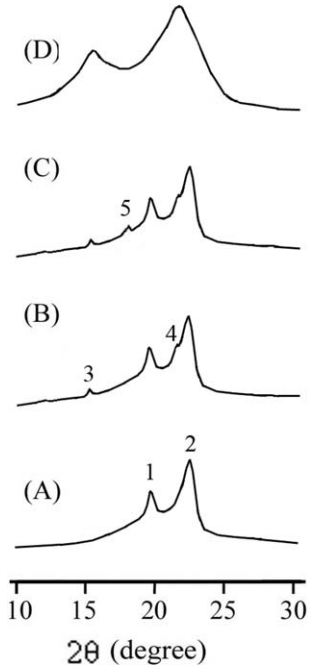

Figure 3 X-ray diffractograms are shown for (A) PBSA, (B) PBSA/SCB (20 wt %), (C) PBSA-*g*-MA/SCB (20 wt %), and (D) SCB.

and is discussed in greater detail in the following sections.

X-ray diffraction

Diffractograms of pure PBSA, PBSA/SCB (20 wt %), PBSA-*g*-MA/SCB (20 wt %), and SCB are shown in Figure 3(A–D). Similar to the results of Ray and Bousmina,[30] pure PBSA [Fig. 3(A)] exhibited two diffraction peaks at about 19.7° and 22.6°, designated 1 and 2, respectively. For the PBSA/SCB composite [Fig. 3(B)], two extra peaks were observed at about 15.2° and 21.6° (designated 3 and 4). The diffractogram of neat SCB also revealed two peaks at 15.2° and 21.6° in Figure 3(D). A comparison of the XRD data obtained on PBSA/SCB and SCB suggests that peaks 3 and 4 may have been caused by physical dispersion of SCB throughout the PBSA matrix. Furthermore, Figure 3(C) shows an additional peak at 18.1° (designated 5) in the diffraction pattern of the PBSA-*g*-MA/SCB composite. This peak, also identified by Danyadi et al.,[31] may have been caused by ester formation. This would indicate that the crystalline structure of the PBSA/SCB composite was altered when PBSA-*g*-MA was used in place of PBSA. Figure 3(D) shows that the neat SCB contained two diffraction peaks at 21.8° and 15.6°. Huang et al.[22] also reported a similar result.

Differential scanning calorimetry test

Differential scanning calorimetry was used to study the thermal properties of blends. Variations in fusion heat (ΔH_f) and melting temperature (T_m) of PBSA/SCB and PBSA-*g*-MA/SCB were determined from the DSC heating thermograms (not shown here), and the results are presented in Table I. In Table I, it can be seen that melting temperature decreased with increasing SCB content for both PBSA/SCB and PBSA-*g*-MA/SCB composites, and that the decrease was more noticeable for SCB content of up to 20 wt %. The lower T_m might be caused by SCB, lowering the melting viscosity of PBSA and PBSA-*g*-MA. The lower melting viscosity of PBSA-*g*-MA/SCB makes composites easier to process than PBSA/SCB.[32]

The values of fusion heat (ΔH_f) of pure PBSA and PBSA-*g*-MA were 50.8 and 48.2 J/g, respectively (Table I). The grafted branches that increased the spacing between the PBSA chains and disrupted the regularity of the chain structure might explain the lower fusion heat of PBSA-*g*-MA.[33] Conversely, as the SCB was composited, we found that PBSA-*g*-MA/SCB gave higher ΔH_f values than PBSA/SCB, with an increment of about 2–9 J/g, a function of the ester carbonyl functional group of PBSA-*g*-MA. However, it was clear that the ΔH_f value, which indicates percentage crystallinity of composites, of both PBSA/SCB and PBSA-*g*-MA/SCB decreased as the content of SCB was increased. These results are similar to those obtained with blends of polyester and natural fibers.[11] Marked decrease in crystallinity of PBSA/SCB composites was probably caused by the increased difficulty in arranging the polymer chain as the SCB prohibited the movements of the polymer segments and by the steric effect caused by the hydrophilic character of SCB, leading to poor adhesion with the hydrophobic PBSA.[11,33]

Composite morphology

In most composite materials, effective wetting and uniform dispersion of all components in a given matrix and strong interfacial adhesion between the phases are required to obtain a composite with satisfactory mechanical properties. In this study, SCB may be thought of as a dispersed phase within a PBSA or PBSA-*g*-MA matrix. To evaluate the composite morphology, SEM was used to examine tensile fractures in

TABLE I
Effect of SCF Content on the Thermal Properties of PBSA/SCF and PBSA-*g*-MA/SCF Composites

	PBSA/SCF		PBSA-*g*-MA/SCF	
SCF (wt %)	T_m (°C)	ΔH_f (J/g)	T_m (°C)	ΔH_f (J/g)
0	87.1	50.8	86.8	48.2
10	86.1	43.6	84.9	45.3
20	85.6	38.3	82.6	43.5
30	85.3	35.1	82.2	42.3
40	85.1	32.6	81.9	41.6

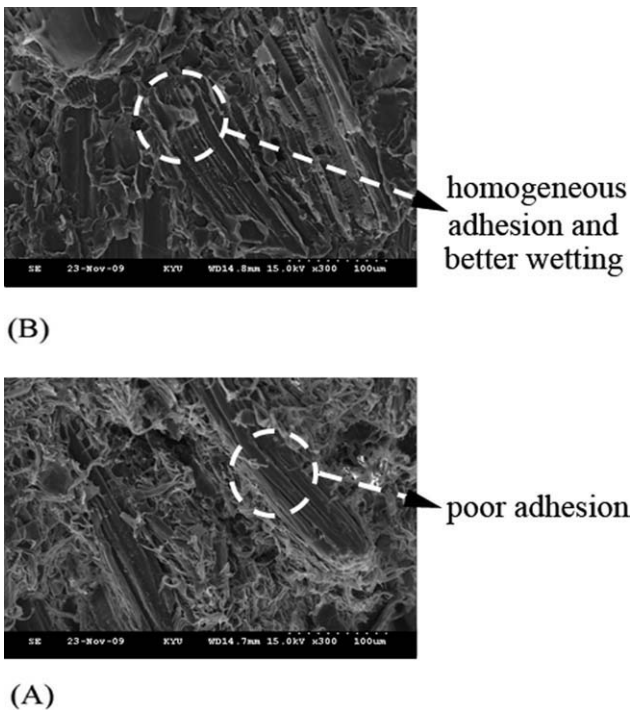

Figure 4 SEM microphotographs show the distribution and wetting of SCB in PBSA/SCB (20 wt %) and PBSA-*g*-MA/SCB (20 wt %) composites.

the surfaces of PBSA/SCB (20 wt %) and PBSA-*g*-MA/SCB (20 wt %) samples. The SEM microphotograph of PBSA/SCB (20 wt %) in Figure 4(A) shows that the SCB in this composite tended to agglomerate into bundles and was unevenly distributed in the matrix. This poor adhesion was due to the formation of hydrogen bonds between SCB fibers and the disparate hydrophilicities of PBSA and SCB. Poor wetting in these composites was also noted [marked in Fig. 4(A)] because of large differences in surface energy between the SCB and the PBSA matrix.[34] The PBSA-*g*-MA/SCB (20 wt %) microphotograph in Figure 4(B) shows a more homogeneous adhesion and better wetting of SCB in the PBSA-*g*-MA matrix, indicated by the complete coverage of PBSA-*g*-MA on the fiber and the removal of both materials when a fiber was pulled from the bulk. This improved interfacial adhesion was due to the similar hydrophilicity of the two components, which allowed for the formation of branched and crosslinked macromolecules, and the prevention of hydrogen bonding between SCB fibers.

Mechanical properties

Figures 5 and 6 show the variations of tensile strength and elongation at break with SCB content for PBSA/SCB and PBSA-*g*-MA/SCB composites. The tensile strength and elongation of pure PBSA (43.1 MPa and 780.6%) decreased after grafting with MA (40.1 MPa and 738.7%). For PBSA/SCB composites (Fig. 5), the tensile strength decreased markedly

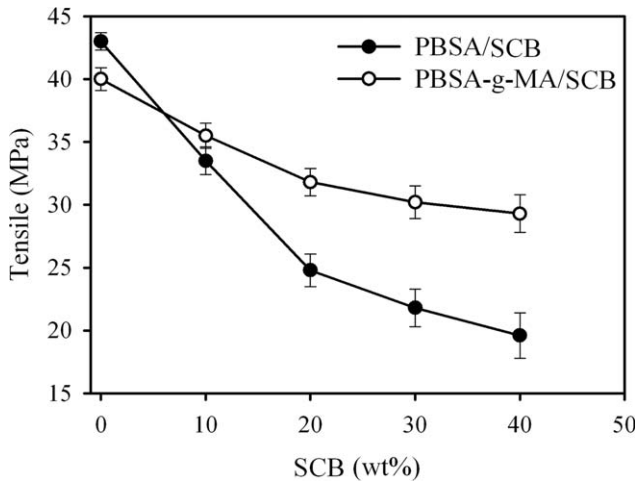

Figure 5 The effect of SCB content on tensile strength at break is shown for PBSA/SCB and PBSA-*g*-MA/SCB composites.

and continuously with increasing SCB content (from 43.1 to 19.7 MPa). This was attributed to poor dispersion of SCB in the PBSA matrix, as previously discussed and as shown in Figure 4(A). The effect of this incompatibility on the mechanical properties of the composites was substantial. The PBSA-*g*-MA/SCB composites in Figure 6 exhibited a unique behavior in regard to the tensile strength at break, which increased with increasing SCB content despite the fact that PBSA-*g*-MA had a lower tensile strength than pure PBSA. Furthermore, the tensile strength of the PBSA-*g*-MA/SCB composites was constant (the decline was tend to slowly) with SCB content beyond 20 wt %. This behavior was likely due to enhanced dispersion of SCB in the PBSA-*g*-MA matrix resulting from the formation of branched or crosslinked marcomolecules.[35] The lower ΔH_f of PBSA-*g*-MA/SCB was likely due to the grafted

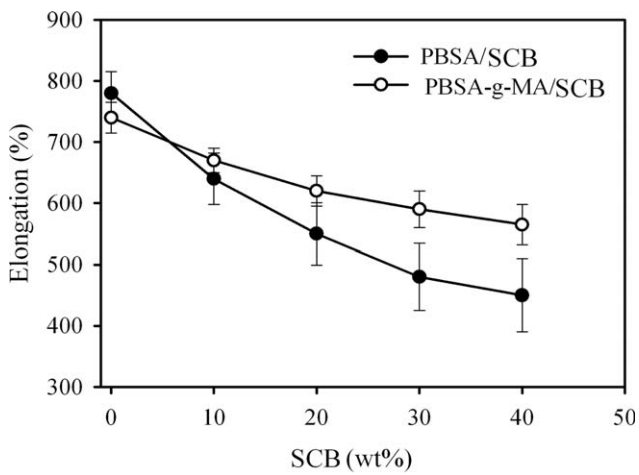

Figure 6 The effect of SCB content on elongation at break is shown for PBSA/SCB and PBSA-*g*-MA/SCB composites.

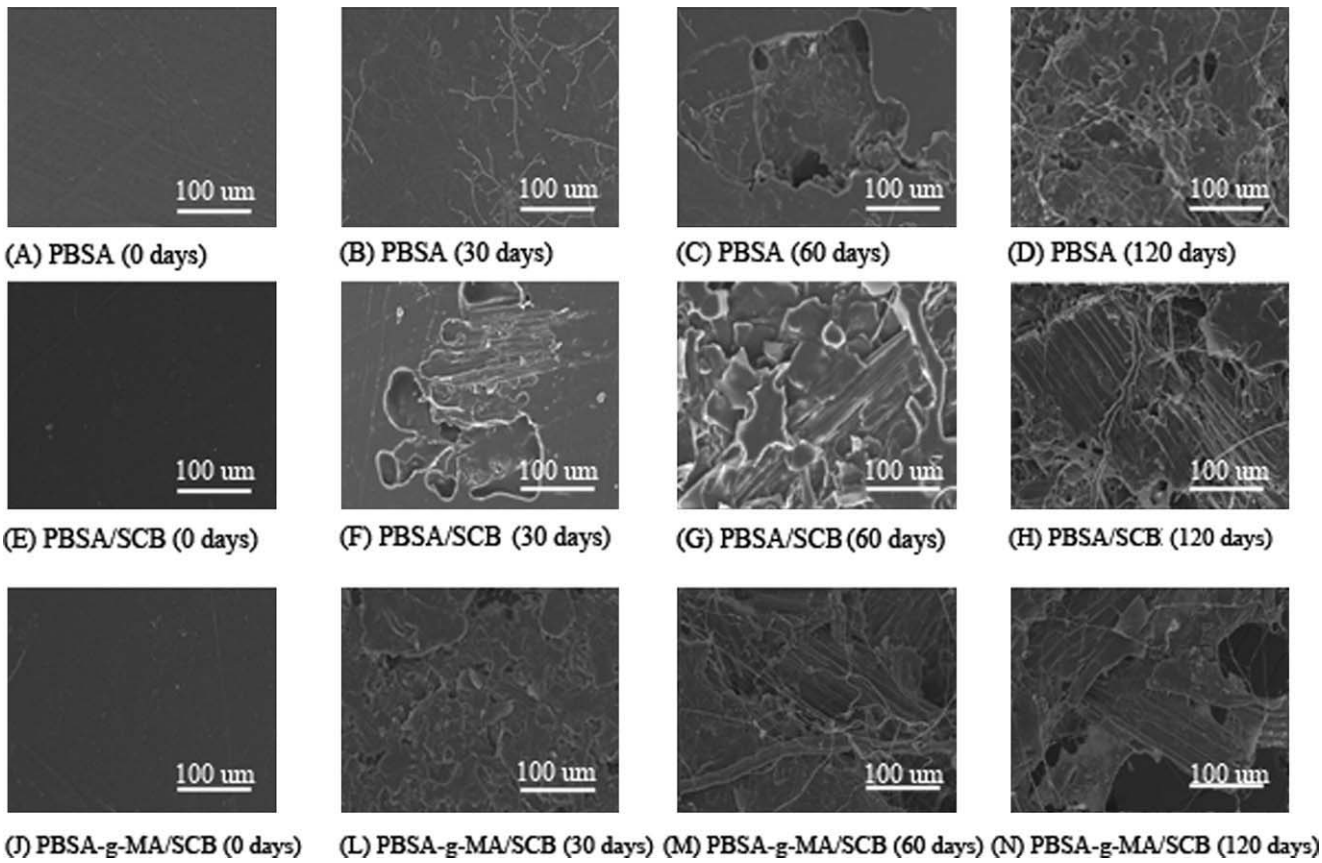

Figure 7 SEM micrographs show the morphology of PBSA (A–D), PBSA/SCB (E–H), and PBSA-*g*-MA/SCB (J–N) films as a function of incubation time in a *Rhizopus oryzae* compost.

branches, which disrupt the regularity of the chain structures in PBSA and increase the spacing between the chains.[36] According to this reason, the tensile strength and elongation decreased when the content of SCB beyond 20 wt % as shown in Figures 5 and 6.

Figure 6 also indicates lower elongation at break values for the PBSA/SCB composites relative to the PBSA-*g*-MA/SCB composites. In PBSA/SCB, the SCB tended to agglomerate into bundles, illustrating the poor compatibility between the two phases. In the PBSA-*g*-MA/SCB composites, as shown in the solid line of Figure 6, the elongation at break also decreased with increasing amounts of SCB but exhibited greater elongation values than did PBSA/SCB composites. However, these values were still lower than those of pure PBSA. These results are similar to those of Wu.[37] The data in Figures 5 and 6 indicate that the grafting reaction in PBSA-*g*-MA/SCB composites improves the tensile strength and elongation of PBSA/SCB. However, the degree of enhancement in elongation is smaller than that in tensile strength.

Biodegradation

Changes in the morphology of both PBSA and PBSA-*g*-MA/SCB composites were noted as a function of the amount of time buried in a *R. oryzae* compost. SEM microphotographs taken after 30, 60, and 120 days in the *R. oryzae* compost illustrate the extent of morphological change (Fig. 7). PBSA/SCB (20 wt %) [Fig. 7(F–H)] exhibited larger and deeper pits that appeared to be more randomly distributed relative to those in the PBSA-*g*-MA/SCB (20 wt %) composites [Fig. 7(L–N)]. These analyses also indicate that biodegradation of the SCB phase in PBSA/SCB (20 wt %) increased with time, confirming the results presented in Figure 8.

After a 30-day incubation period, cell growth with gradual erosion and cracking was observed on the surface of the PBSA matrix [Fig. 7(B)]. After 60 days, the disruption of the PBSA matrix structure became more obvious [Fig. 7(C)]. This degradation was confirmed by increasing weight loss of the PBSA matrix with incubation time (Fig. 8), which reached nearly 18% after only 60 days. The most likely cause of this weight loss was biodegradation by *R. oryzae*. Bacterial degradation of PBSA has been previously reported,[6,38] and some have described degradation mechanisms involving enzymes such as lysozyme.[39,40] The results shown here indicate that *R. oryzae* is very effective at degrading PBSA.

The SEM micrographs in Figure 7 indicate that the PBSA-*g*-MA/SCB (20 wt %) composites were more

easily degraded than was pure PBSA. After a 20-day incubation period, the PBSA-*g*-MA/SCB composite was coated with a biofilm of bacterial cells [Fig. 7(L)], indicating more cell growth than on PBSA at the same incubation time. Moreover, at 60 and 120 days, larger pores were apparent on the PBSA-*g*-MA/SCB composite [Fig. 7(M,N)], indicating a higher level of degradation. The degree of weight loss of the PBSA-*g*-MA/SCB composites was also accelerated relative to that of PBSA, exceeding 40% after 60 days (Fig. 8). These results clearly demonstrate that the addition of SCB to the MA-grafted PBSA enhanced the biodegradability of the composite.

Figure 8 shows the percentage weight change as a function of time for PBSA/SCB and PBSA-*g*-MA/SCB composites buried in the *R. oryzae* compost. For both composites, the degree of weight loss increased with SCB content. Composites with 40% SCB degraded rapidly over the first 60 days, losing a mass equivalent to their approximate SCB content, and showed a gradual decrease in weight over the next 60 days. PBSA-*g*-MA/SCB exhibited a weight loss of $\sim$ 3–8 wt %.

Intrinsic viscosity

The change in intrinsic viscosity and molecular weight as a function of incubation time for PBSA and the PBSA-*g*-MA/SCB composites is shown in Figure 9. The intrinsic viscosity for PBSA with encapsulated *R. oryzae* ranged from 2.61 to 1.25 g/dL over the 120-day incubation period. The corresponding changes for PBSA-*g*-MA/SCB were 2.47–0.78 g/dL. The lower intrinsic viscosity of the latter suggests a higher degree of polymer fragmentation. Additionally, the decreased intrinsic viscosity of PBSA-*g*-MA/SCB may be due to conformational changes in the SCB fiber caused by the previously discussed formation of ester groups. These

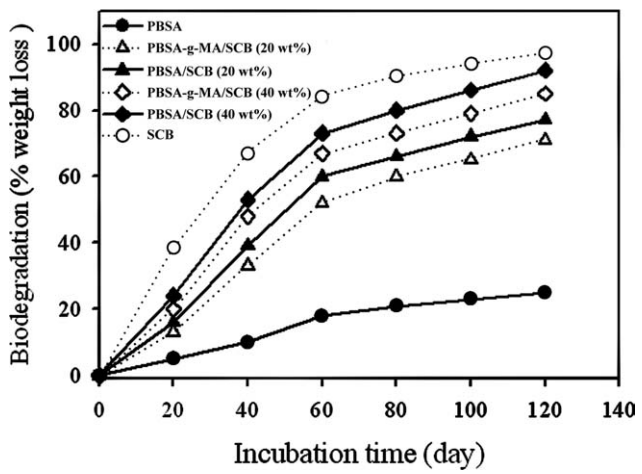

Figure 8 Weight loss percentages of PBSA, PBSA/SCB, and PBSA-*g*-MA/SCB are shown as a function of incubation time in a *Rhizopus oryzae* compost.

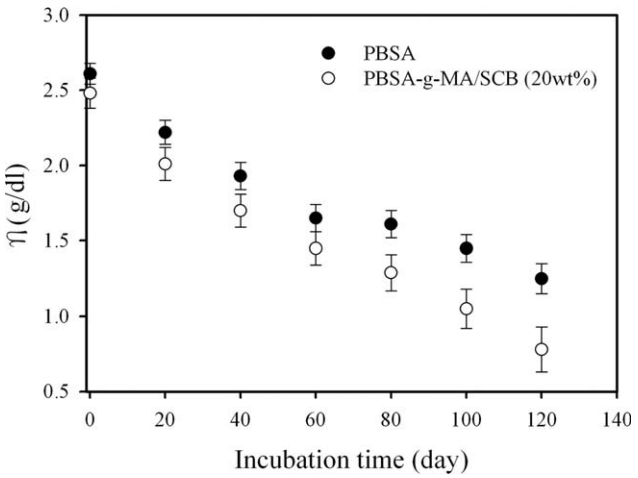

Figure 9 The intrinsic viscosity is plotted as a function of incubation time for PBSA and PBSA-*g*-MA/SCB loaded with *Rhizopus oryzae*.

results corroborate the findings of Singh et al.,[41] which showed that the intrinsic viscosity of esterified PBSA fell with an increase in random hydrolysis of the ester group during biodegradation.

CONCLUSIONS

The compatibility and mechanical properties of SCB blended with PBSA and MA-modified PBSA (PBSA-*g*-MA) were examined. FTIR, NMR, and XRD analyses revealed the formation of ester groups due to reactions between —OH groups in SCB and anhydride carboxyl groups in PBSA-*g*-MA, significantly altering the crystal structure of the composite material. The melting temperature (T_m) and fusion heat (ΔH_f) of PBSA/SCB decreased with increasing SCB content, whereas that of PBSA-*g*-MA/SCB increased. The morphology of PBSA-*g*-MA/SCB composites was consistent with good adhesion between the SCB phase and the PBSA-*g*-MA matrix. In mechanical tests, PBSA-*g*-MA enhanced the mechanical properties of the composite because of the good adhesion, especially the tensile strength. The biodegradation rate of PBSA-*g*-MA/SCB was lower than that of PBSA/SCB but higher than that of pure PBSA, when incubated with *R. oryzae.* After 120 days, the PBSA-*g*-MA/BF (40 wt %) composite suffered a greater than 80% weight loss. The degree of biodegradation increased with increasing SCB content. Decreases in intrinsic viscosity were also greater for SCB composites, suggesting a strong connection between biodegradability and these characteristics.

References

1. Choi, M. C.; Kim, Y.; Ha, C. S. Prog Polym Sci 2008, 33, 581.
2. Rosa, I. M. D.; Santulli, C.; Sarasini, F. Compos Part A: Appl Sci Manuf 2009, 40, 1456.

3. Dobircau, L.; Sreekumar, P. A.; Saiah, R.; Leblanc, N.; Terrié, C.; Gattin, R.; Saiter, J. M. Compos Part A: Appl Sci Manuf 2009, 40, 329.
4. Bogoeva-Gaceva, G.; Avella, M.; Malinconico, M.; Buzarovska, A.; Grozdanov, A.; Gentile, G.; Errico, M. E. Polym Compos 2007, 28, 98.
5. Reddy, N.; Yang, Y. Polym Eng Sci 2009, 49, 2212.
6. Zhao J. H.; Wang, X. Q.; Zeng, J.; Yang, G. Polym Degrad Stab 2005, 90, 173.
7. Rattoa, J. A.; Stenhousea, P. J.; Auerbacha, M.; Mitchellb, J.; Farrellb, R. Polymer 1999, 40, 6777.
8. Correlo, V. M.; Boesel, L. F.; Bhattacharya, M.; Mano, J. F.; Neves, N. M.; Reis, R. L. Mater Sci Eng A 2005, 403, 57.
9. El-Tayeb, N. S. M. Wear 2008, 265, 223.
10. Singh, S.; Mohanty, A. K. Compos Sci Technol 2007, 67, 1753.
11. Wu, C. S. Polym Degrad Stab 2009, 94, 1076.
12. Houda, B.; Barbara, R.; Mohamed, M. Bioresour Technol 2009, 100, 6537.
13. Satyanarayana, K. G.; Arizaga, G. G. C.; Wypych, F. Prog Polym Sci 2009, 34, 982.
14. Idicula, M.; Boudenne, A.; Umadevi, L.; Ibos, L. Compos Sci Technol 2006, 66, 2719.
15. Khalil, H. P. S. A.; Ismail, H. Polym Test 2000, 20, 65.
16. Wang, K. H.; Wu, T. M.; Shih, Y. F.; Huang, C. M. Polym Eng Sci 2008, 48, 1833.
17. Ahn, B. D.; Kim, S. H.; Kim, Y. H.; Yang, J. S. J Appl Polym Sci 2002, 82, 2808.
18. Edlund, U.; Albertsson, A. C. Adv Drug Delivery Rev 2003, 55, 585.
19. Ha, C. S.; Cho, W. J. Prog Polym Sci 2002, 27, 759.
20. Quentin, B.; Magali, F.; Michel, G. Appl Surf Sci 2007, 253, 4753.
21. Ahn, B. D.; Kim, S. H.; Kim, Y. H.; Yang, J. S. J Appl Polym Sci 2001, 82, 2808.
22. Huang, Z.; Liang, X.; Hu, H.; Gao, L.; Chen, Y.; Tong, Z. Polym Degrad Stab 2009, 94, 1737.
23. Vieira, J. G.; Oliveira, G. C.; Filho, G. R.; Assuncao, R. M. N.; Meireles, C. S.; Cerqueira, D. A. Carbohydr Polym 2009, 78, 779.
24. Wu, C. S. Polym Degrad Stab 2003, 80, 127.
25. Yin, J.; Zhang, J.; Yao, Y. J Appl Polym Sci 2006, 102, 841.
26. Wang, Q.; Qi, R.; Shen, Y.; Liu, Q.; Zhou, C. J Appl Polym Sci 2007, 106, 3220.
27. Viera, R. G. P.; Filho, G. R.; Assunc, R. M. N.; Meireles, C. S. Carbohydr Polym 2007, 67, 182.
28. Yoshimura, T.; Yoshimura, R.; Seki, C.; Fujioka, R. Carbohydr Polym 2006, 64, 345.
29. Gayload, N. G.; Nagler, M.; Watterson, A. C. Eur Polym J 1983, 19, 877.
30. Ray, S. S.; Bousmina, M. Polymer 2005, 46, 12430.
31. Danyadi, L.; Janecska, T.; Szabo, Z.; Nagy, G.; Moczo, J.; Pukanszky, B. W. Compos Sci Technol 2007, 67, 2838.
32. Wu, C. S. J Appl Polym Sci 2006, 102, 3565.
33. Aburto, J.; Thiebaud, S.; Alric, I.; Bikiaris, D.; Prinos, J.; Panayioyou, C. Carbohydr Polym 1997, 34, 101.
34. Abdul-Khalil, H. P. S.; Ismail, H. Polym Test 2001, 20, 65.
35. Bikiaris, D.; Prinos, J.; Koutsopoulos, K.; Vouroutzis, N.; Pavlidou, E.; Frangi, N.; Panayiotou, C. Polym Degrad Stab 1998, 59, 287.
36. Radiman, C.; Yuliani, G. Polym Int 2008, 57, 502.
37. Wu, C. S. J Appl Polym Sci 2010, 115, 948.
38. Kim, H. S.; Kim, H. J.; Lee, J. W.; Choi, I. G. Polym Degrad Stab 2006, 91, 1117.
39. Ishii, N.; Inoue, Y.; Tagaya, T.; Mitomo, H.; Nagai, D.; Kasuya, K. I. Polym Degrad Stab 2008, 93, 883.
40. He, Y.; Asakawa, N.; Masuda, T.; Cao, A.; Yoshie, N.; Inoue, Y. Eur Polym J 2000, 36, 2221.
41. Singh, R. P.; Pandey, J. K.; Rutot, D.; Dege'e, P.; Duboisb, P. Carbohydr Res 2003, 338, 1759.